

Hierarchical Generative Network for Face Morphing Attacks

Zuyuan He, Zongyong Deng, Qiaoyun He and Qijun Zhao*
College of Computer Science, SiChuan University, Chengdu, China

Abstract—Face morphing attacks circumvent face recognition systems (FRSs) by creating a morphed image that contains multiple identities. However, existing face morphing attack methods either sacrifice image quality or compromise the identity preservation capability. Consequently, these attacks fail to bypass FRSs verification well while still managing to deceive human observers. These methods typically rely on global information from contributing images, ignoring the detailed information from effective facial regions. To address the above issues, we propose a novel morphing attack method to improve the quality of morphed images and better preserve the contributing identities. Our proposed method leverages the hierarchical generative network to capture both local detailed and global consistency information. Additionally, a mask-guided image blending module is dedicated to removing artifacts from areas outside the face to improve the image's visual quality. The proposed attack method is compared to state-of-the-art methods on three public datasets in terms of FRSs' vulnerability, attack detectability, and image quality. The results show our method's potential threat of deceiving FRSs while being capable of passing multiple morphing attack detection (MAD) scenarios.

I. INTRODUCTION

Face Recognition Systems (FRSs) [3,12,14,32] have been extensively deployed in critical security applications, such as Automatic Border Control (ABC) and financial services. However, FRSs can be vulnerable to various attacks like face forgery, and face morphing attacks [4,34]. Where the face morphing attack is to create an image with multiple identities. Ferrara *et al.* [22] demonstrated that a single face morphing attack image can successfully match with more than one person, disrupting the one-to-one mapping between original face images and individual identity. To better protect FRSs from morphing attacks, it is important to understand how to generate high quality morphing attack images, especially considering the recent rapid advances in generative models.

In the literature, face morphing methods can be divided into two categories: landmark-based [21,28,29] and generation-based [1,8,10,18,35,38]. Landmark-based morphing methods create face morphing attacks on the image level, usually by interpolating the contributors' facial landmarks to perform Delaunay triangulation, warping the contributing images to align the interpolated average landmarks, and then alpha blending the two warped images to obtain the morphed image. Such methods are excellent at preserving the identity of the contributing images and pose a greater threat to FRSs. Nevertheless, artifacts like blurring and ghosting are created

in areas around the eyes, nose, mouth, and hair due to insufficient landmarks detection during morphing. To alleviate artifacts, existing landmark-based morphing methods resort to additional post-processing steps. ReGenMorph [9] uses Generative Adversarial Networks (GAN) as a post-processing module to remove blending artifacts and gets visibly realistic morphed images. However, it greatly decreased the attack capability of the morphed images. Hence, while ensuring the attack capability of morphs, improving their visual quality further remains a challenge.

Unlike landmark-based methods, the generation-based methods are performed on the latent level. The contributing images are projected into the latent space, and their identities are interpolated to synthesize the morphed images. Such morphs exhibit improved visual quality, yet minor artifacts persist. However, these methods do not effectively preserve the identities of contributing images. Most of these methods rely on a single network to extract global information, such as shapes and textures. Local information that can better capture subtle facial features and variations is ignored, for instance, the color of the eyes or the shape of the nose and mouth [2,27]. This motivates us to use GANs with different structures to extract both global and local information from contributing images, facilitating the generation of morphs that are more threatening to FRSs.

In this paper, we propose an end-to-end Hierarchical Generative network for Face Morphing (HGFM) attacks. Fig. 1 highlights the main difference between our method and existing ones. Traditional landmark-based methods suffer from solid artifacts outside the facial area when landmarks are missing, while generation-based methods sacrifice detailed biometrics and produce blurry morphs. In contrast, our method effectively extracts local detailed and global consistency information from facial images, resulting in morphs with better visual quality. The principal contributions of this paper are outlined as follows:

- We devise a hierarchical structure comprising one global morph network and six local morph networks to extract local and global information for morphed face image generation.
- We design a loss function with five loss terms, including a novel combined identity loss (to improve the generalization ability of morphed images) and a geometry loss (to preserve the face geometric information of both contributors).
- We propose a mask-guided image blending module that effectively removes artifacts to improve the visual quality and preserve identity better.

*Corresponding author

This work is supported by the National Natural Science Foundation of China (No. 61773270, 62176170).

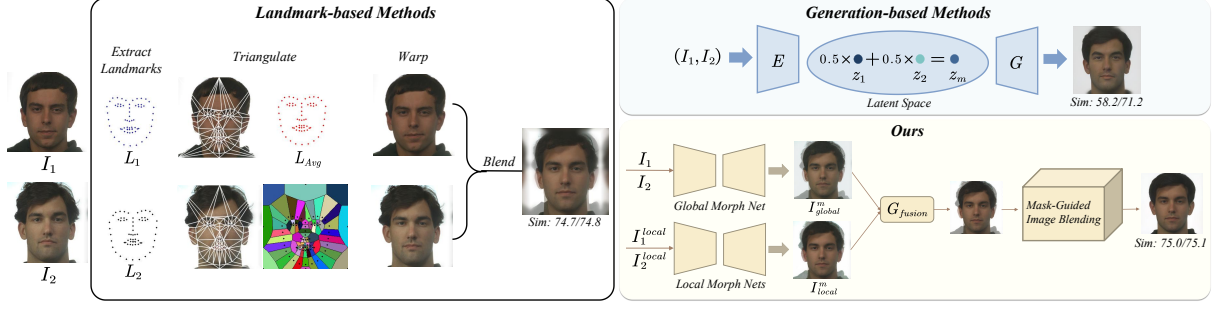


Fig. 1. Illustration of different face morphing methods. ‘Sim’ denotes the similarity between morphed and contributing images, which is computed by using ElasticFace [3].

We evaluate the proposed HGFM on three face datasets and compare them to publicly available state-of-the-art morphing methods. The results demonstrate that HGFM generates morphed images with favorable visual quality, better identity preservation, and a higher threat to FRSS.

II. RELATED WORK

A. Face Morphing Attacks

Existing face morphing attacks are performed either on image-level or on latent-level. Landmark-based morphing methods create face morphing attacks on image-level, and the morphed images are obtained by interpolating facial landmarks and blending the texture. Among the open-source face morphing, GIMP/GAP, OpenCV [21], and FaceMorpher [28] rely on landmarks. The morphs generated by these methods have apparent artifacts that appear unrealistic and easily detectable by human observers. ReGenMorph [9] used an additional GAN to eliminate artifacts. In [27], it introduced a partial face manipulation-based morphing method that only focuses on two specific regions (eyes and nose). However, this is tedious and reduces the performance of morphs. Generation-based morphing methods typically use generation models like GAN and diffusion models to create morphed images by merging two facial images on the latent level. MorGAN, proposed by Damer *et al.* [10], was the first to use GAN to generate morphs with minor artifacts, which can not preserve identity well and are limited in low resolution (64×64 pixels). Later, Damer *et al.* [7] proposed an image enhancement solution to increase the quality and resolution of GAN-based morphs. Inspired by MorGAN, Venkatesh *et al.* [35] used StyleGAN [18] to generate realistic morphs with both high quality and high resolution (1024×1024 pixels). Then, MIPGAN-I and MIPGAN-II [38] used the StyleGAN architecture to generate morphs with improved identity preservation by introducing a novel loss function. Recently, Blasingame [1] and Damer *et al.* [8] investigated using diffusion models to create morphs. He *et al.* [13] produced high realistic morphs by optimizing morphing landmarks and using Graph Convolutional Networks (GCNs) to combine landmarks and appearance features.

B. Image Blending

Image blending is widely used as a post-processing method to remove artifacts from morphed images. It involves

taking a specific area from one image and seamlessly integrating it into a specific location in another image to create a composite image that appears natural. As described in [26], Poisson image blending is a widely employed technique for achieving smooth gradient transitions in composite images. Inspired by this work, we use a mask to identify the face region and separate it from the background region like hair and clothes in morphed images with visible artifacts. Then, we blend the morphed face with an auxiliary image (background image) to remove artifacts outside the face region.

III. METHODOLOGY

A. Overview of HGFM

A high-level overview of HGFM is presented in Fig. 2. Our model uses multiple constraints to generate morphed images end-to-end through a hierarchical structure. The morphing process in HGFM can be roughly divided into the following steps:

Initialization. Given two bona fide images denoted as I_1 and I_2 , a landmark morphed image I_{land}^m is generated by OpenCV [21] morphing algorithm. This provides us with facial geometry information for morphing process. In addition, I_1 and I_2 are embedded into the latent space of a pre-trained StyleGAN2 encoder E to obtain the corresponding latent codes w_1 and w_2 . Then the latent codes are combined using a morph factor of 0.5 and fed into the StyleGAN2 generator G to generate an auxiliary morphed image I_{aux}^m .

Stage-I: Face Morphing. At this step, the global morphed image I_{global}^m and the local morphed image I_{local}^m are generated by global and local morph networks, respectively. Then the fusion network G_{fusion} fuses I_{global}^m and I_{local}^m together to obtain the intermediate morphed image I_M .

Stage-II: Mask-Guided Image Blending. We use the face parser S to get face masks M_m^{face} and M_{aux}^{face} for I_M and I_{aux}^m . During the blending step, the M_m^{face} is used as the blending mask to combine I_M with I_{aux}^m together to generate the final morphed image I_M' .

B. Framework Architecture

HGFM is established on two separate modules to achieve the generation of morphed images: (i) the hierarchical GAN for face morphing, and (ii) a mask-guided image blending module used to eliminate visible artifacts.

Stage-I: The Hierarchical GAN for Face Morphing

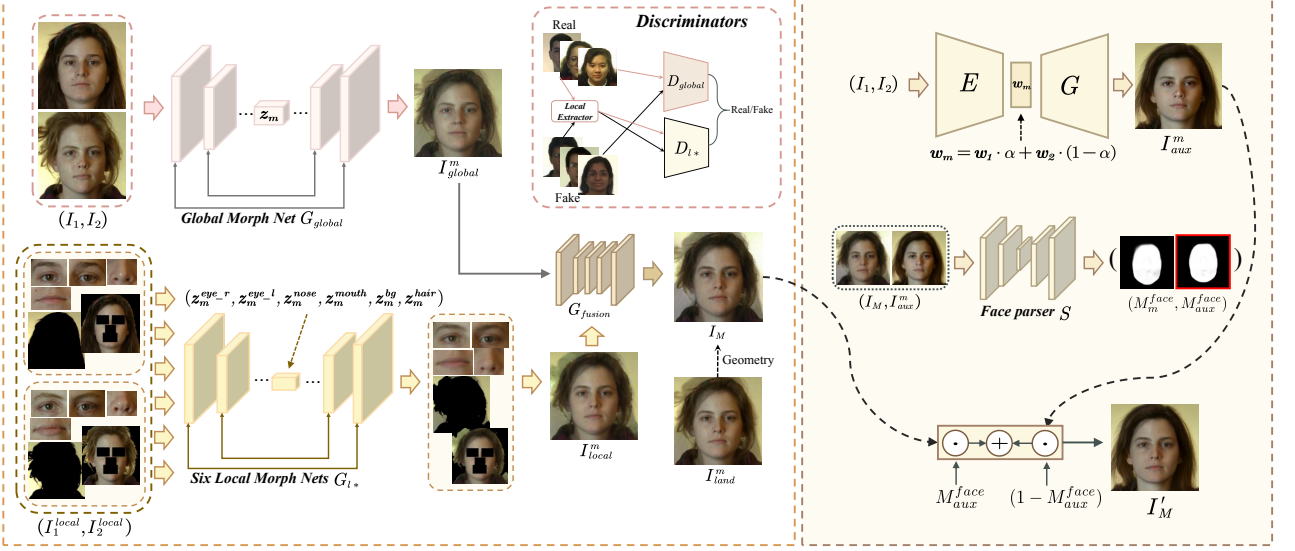


Fig. 2. Overview of the proposed HGFM method. It consists of two modules, the hierarchical GAN for face morphing and mask-guided image blending. The former uses hierarchical generative network containing a global morph net G_{global} and six local morph nets G_{l*} to generate a global morphed image I_{global}^m and a local morphed image I_{local}^m , respectively, and then fuse them to obtain an intermediate morphed image I_M . The latter uses a pre-trained StyleGAN2 model to generate an auxiliary morphed image I_{aux}^m , and the face parser is used to define the face masks M_m^{face} and M_{aux}^{face} of I_M and I_{aux}^m for image blending. The final result I_M' is generated by combining I_M and I_{aux}^m according to M_{aux}^{face} .

1) *The Hierarchical GAN for Face Morphing*: Different from the standard GAN architecture, our proposed hierarchical structure targets both *hierarchical generator* and *hierarchical discriminator*, each containing a global network and six local networks. The global network analyzes and processes the holistic face image to extract global consistency information. Since the facial region contains richer identity information, we utilize six local networks to extract the subtle features of the eyes, nose, mouth, and other effective facial regions. During the morphing process, we not only perform a global fusion of the contributing identities, but also consider the varying levels of importance of different facial regions in recognition. Accordingly, we fuse contributing subjects' facial regions separately. The hierarchical structure aims to overcome the limitations of a single network by efficiently extracting features from face images with diverse regions.

Hierarchical Generator. In the hierarchy of $G = \{G_{global}, G_{l*}, G_{fusion}\}$, G_{global} is the global generator, $G_{l*} = \{G_{eye.l}, G_{eye.r}, G_{nose}, G_{mouth}, G_{bg}, G_{hair}\}$ is a set of six local generators, and G_{fusion} is a fusion network. The U-Net structure is used to build all of the generators. G_{global} is a U-Net with eight down-convolutional and eight up-convolutional blocks. It extracts similar shape and texture features from the contributing images to fuse them effectively. Each of $G_{eye.l}$, $G_{eye.r}$, G_{nose} , and G_{mouth} is a U-Net with three down-convolutional and three up-convolutional blocks. We use MTCNN [39] to detect the central landmarks of each facial region (i.e., left eye, right eye, nose and mouth). Based on these landmarks, we extract pairs of facial region patches from the image pair (I_1, I_2) . For each patch pair, we use a linear combination of them to obtain the

average facial region patch $(z_m^{eye.l}, z_m^{eye.r}, z_m^{nose}, z_m^{mouth})$. Then, we feed them into the corresponding local generator G_{l*} to generate a set of intermediate states for local morphed patches. Each local generator captures detailed information on facial regions such as eye color, mouth shape and so on. This compensates for the limitations of the global network, which cannot capture such fine-grained details. Each of G_{bg} and G_{hair} is a U-Net with four down-convolutional and four up-convolutional blocks. The background regions in I_1 and I_2 are detected using the portrait segmentation method [19] and interpolated to obtain z_m^{bg} , which is input to G_{bg} . The remaining region of I_1 and I_2 are interpolated together to obtain z_m^{hair} as an input to G_{hair} . All the outputs of local generators are combined to make a complete local morphed image I_{local}^m . This image reattaches facial region patches based on the central landmarks detected by MTCNN [39] and addresses overlapping regions through minimum pooling. Additionally, the generator includes a fusion network G_{fusion} , which comprises a flat convolutional module block, three residual blocks, and a final convolutional layer. This network is responsible for synthesizing the global and local morphed images, I_{global}^m and I_{local}^m , to generate the intermediate morphed image I_M .

Hierarchical Discriminator. The role of the discriminator is to distinguish between real and fake input images. In the hierarchy of $D = \{D_{global}, D_{l*}\}$, D_{global} is a global discriminator, and $D_{l*} = \{D_{eye.l}, D_{eye.r}, D_{nose}, D_{mouth}, D_{bg}, D_{hair}\}$ is a set of six local discriminators. D_{global} uses multi-scale discriminator in Pix2PixHD [36] to examine the entire image and extract multiple layers of features from the real and fake

images. D_{l*} uses Markovian discriminator in Pix2Pix [16] to examine distinct local facial regions to evaluate the quality of fine details. The Markovian discriminator process every 70×70 patch of the input image and evaluates the style of each patch, enabling the discriminator to learn local patterns at various levels of granularity, such as coarse and fine levels of the local input. This procedure can better distinguish bona fide images from morphed images.

2) *The Mask-Guided Image Blending*: Existing morphing methods, either landmark-based or generation-based methods, do not carefully consider the impact of non-face regions in contributing face images, resulting in ghost artifacts in morphed images. To address the noticeable artifacts present in areas such as hair, ears, and neck in the morphed images generated by the first module, we incorporate a mask-guided blending network. This network effectively removes these artifacts and ensures the production of visibly realistic morphed images. First, we use a pre-trained StyleGAN2 model to generate an auxiliary morphed image I_{aux}^m . Then, as shown in Fig. 2, we use a face parser S based on DeepLabV3 [5] to predict the face components of the image. Formally, the model implements a mapping from an image to a tensor of probabilities along the channel dimension, *i.e.*: $S : \mathbb{R}^{3 \times n \times m} \rightarrow [0, 1]^{L \times n \times m}$, where L is the number of face components. The face mask M^{face} of image I includes several effective facial regions and is calculated as follows:

$$M^{face}(I) = S_{skin}(I) + S_{eyes}(I) + S_{nose}(I) + S_{eyebrows}(I) + S_{mouth}(I). \quad (1)$$

The face masks (M_m^{face} and M_{aux}^{face}) are calculated individually for the intermediate morphed image I_M and the auxiliary morphed image I_{aux}^m by (1). We take I_M as the foreground image, I_{aux}^m as the background image, and M_{aux}^{face} as the blending mask. The final morphed image I'_M is generated as (2). During the blending stage, the facial regions of I_M and I_{aux}^m may have different sizes, causing artifacts in the facial contours of I'_M . Therefore, we propose a mask loss (see (5)) to solve this problem.

$$I'_M = M_{aux}^{face} \odot I_M + (1 - M_{aux}^{face}) \odot I_{aux}^m. \quad (2)$$

C. Loss Function

During the training stage, multiple loss terms are employed to optimize the morphing process. These loss terms include the geometry loss \mathcal{L}_{gm} , the combined identity loss \mathcal{L}_{cid} , the mask loss \mathcal{L}_{mask} , the appearance loss \mathcal{L}_{app} , and the adversarial loss \mathcal{L}_{adv} .

Geometry Loss. Previous studies [9,35] suggest that morphed images produced by generation-based methods often lose significant facial geometric information, whereas landmark-based methods preserve the geometric information of the contributing subjects well. Being aware of this, we propose to use landmark-based morphed images to supervise the generation of morphed images at the pixel-level. By leveraging the rich information contained in the landmark-based morphed images to guide the creation of morphed

images with greater fidelity. The geometry loss can be written as below.

$$\mathcal{L}_{gm} = \|I_M - I_{land}^m\|_1, \quad (3)$$

where we use the L_1 norm to measure the pixel loss between the intermediate morphed image and the landmark morphed image.

Combined Identity Loss. Previous studies [10,38] only used a single pre-trained face recognition (FR) model to calculate the identity loss. Unlike the standard identity loss, we propose to use multiple FR models to jointly calculate the identity loss between the intermediate morphed image I_M and the two contributing images, using ArcFace [12] and FaceNet [32], respectively. This strategy aims to improve the generalization ability of our morphing method under known and unknown FR techniques. The combined identity loss is formulated as follows:

$$\mathcal{L}_{cid} = \frac{d(z_m^a, z_1^a) + d(z_m^a, z_2^a)}{2} + \frac{d(z_m^f, z_1^f) + d(z_m^f, z_2^f)}{2}, \quad (4)$$

where $d(\cdot)$ denotes the cosine distance function, z_*^a and z_*^f are the features extracted by ArcFace [12] and FaceNet [32] respectively.

Mask Loss. Differences in facial region sizes between the intermediate morphed image I_M and the auxiliary morphed image I_{aux}^m can result in visible artifacts around the face during blending, impacting image quality. To address this, we introduce the mask loss following [23].

$$\mathcal{L}_{mask} = \|M_m^{face} - M_{aux}^{face}\|_2^2. \quad (5)$$

Appearance Loss. To enrich the texture details of the contributing images within the morphed image, we employ an appearance loss comprising a perceptual loss [38], a weak feature matching loss [6], and a local loss [37]. The loss function is formulated as below.

$$\mathcal{L}_{app} = \mathcal{L}_{per} + \mathcal{L}_{wfm} + \mathcal{L}_{local}. \quad (6)$$

Adversarial Loss. The adversarial loss term consists of two parts: the Hinge version adversarial loss for global adversarial loss $\mathcal{L}_{adv}^{global}$ and the BCE version adversarial loss for local adversarial loss $\mathcal{L}_{adv}^{local}$. The adversarial loss is formulated as below.

$$\begin{aligned} \mathcal{L}_{adv}^{global} &= \mathbb{E}_{x \sim X} [\max(0, 1 - D(x))] \\ &\quad + \mathbb{E}_{y \sim Y} [\max(0, 1 + D(y))] - \mathbb{E}_{y \sim Y} [D(y)], \\ \mathcal{L}_{adv}^{local} &= \sum_{D_j \in D_{l*}} \mathbb{E}_{(x_i) \sim X} [\log(D_j(x_i))] \\ &\quad + \mathbb{E}_{(y_i) \sim Y} [\log(1 - D_j(y_i))], \\ \mathcal{L}_{adv} &= \mathcal{L}_{adv}^{global} + \mathcal{L}_{adv}^{local}, \end{aligned} \quad (7)$$

where x is the real images, y is the generated morphed images, x_i is the i -th face region of the real image, and y_i is the i -th face region of the morphed image.

Thus, the overall loss function can be formulated as:

$$\mathcal{L}_{all} = \lambda_1 \mathcal{L}_{gm} + \lambda_2 \mathcal{L}_{cid} + \lambda_3 \mathcal{L}_{mask} + \lambda_4 \mathcal{L}_{app} + \lambda_5 \mathcal{L}_{adv}, \quad (8)$$

TABLE I

COMPARISON OF MMPMR@FMR=0.1%, FID, SSIM AND PSNR VALUES OF OUR APPROACH WITH OTHER METHODS ON FERET, FRLL, AND FRGC DATASETS. FN, AF, CF, AND EF DENOTE FACENET, ARCFACE, CURRICULARFACE, AND ELASTICFACE, RESPECTIVELY. BEST RESULTS ARE SHOWN IN BOLD.

Dataset	Method	FID↓	SSIM↑	PSNR↑	MMPMR (%)↑			
					FN [32]	AF [12]	CF [14]	EF [3]
FERET	FaceMorpher [28]	56.5	0.5860	12.91	58.6	83.2	91.7	84.7
	OpenCV [21]	53.8	0.6278	14.63	58.4	85.3	93.7	86.2
	StyleGAN2 [35]	38.3	0.6360	14.71	18.0	24.1	14.4	7.9
	MIPGAN-II [38]	41.2	0.6411	14.94	47.3	53.4	68.4	54.7
	ReGenMorph [9]	58.6	0.6921	16.60	45.7	77.3	81.7	72.8
	MorDIFF [8]	56.8	0.6668	15.93	47.2	78.6	83.9	79.9
	HGFM (Ours)	40.5	0.6756	15.15	59.9	85.8	93.4	88.9
FRLL	FaceMorpher [28]	81.2	0.6198	15.10	92.8	98.4	99.6	99.4
	OpenCV [21]	69.7	0.6754	17.01	90.8	99.5	99.4	99.6
	StyleGAN2 [35]	36.1	0.6786	17.09	37.6	78.7	63.5	57.2
	MIPGAN-II [38]	37.5	0.7036	17.41	82.9	81.9	90.1	89.9
	ReGenMorph [9]	58.0	0.7213	19.33	84.5	97.4	99.1	98.0
	MorDIFF [8]	49.4	0.7356	18.73	82.6	96.7	98.8	98.8
	HGFM (Ours)	33.7	0.7013	17.90	93.5	99.1	99.9	99.9
FRGC	FaceMorpher [28]	76.9	0.6903	20.30	82.7	96.7	97.8	96.7
	OpenCV [21]	68.3	0.7208	20.96	81.0	96.0	97.6	96.1
	StyleGAN2 [35]	73.4	0.6749	19.27	23.6	53.6	35.2	26.0
	MIPGAN-II [38]	87.1	0.6739	19.21	77.0	77.7	88.2	81.4
	ReGenMorph [9]	98.5	0.7264	21.14	68.3	92.6	88.9	88.9
	MorDIFF [8]	93.8	0.7339	20.88	66.2	95.0	95.8	94.2
	HGFM	88.4	0.7408	20.32	86.2	96.1	98.9	98.3

where $\lambda_1, \lambda_2, \lambda_3, \lambda_4$ and λ_5 are the hyper-parameters that are set to achieve stable and generalized convergence. In this work, we set $\lambda_1, \lambda_2, \lambda_3, \lambda_4 = 10, \lambda_5 = 1$, respectively.

IV. EXPERIMENTS

A. Implementation details

For each face image, we extract 68 landmarks and then align and crop the face images according to the FFHQ [18] process, with input image size 256×256 . Our model is trained on one GeForce RTX 2080 Ti with batch size 1. We use an Adam optimizer with a fixed learning rate of 2×10^{-4} to optimize the network.

B. Datasets and Evaluation Metrics

Datasets. In this paper, we use the FERET [25], FRLL [11], and FRGC [24] face datasets to generate morphed images. To compare with previous work, we employ FERET-Morphs, FRLL-Morphs, and FRGC-Morphs [30], each morph dataset contains four types of morphing attacks, namely FaceMorpher [28], OpenCV [21], StyleGAN2 [35] and MIPGAN-II [38]. The number of images generated by each morphing method is the same as in [17]. In order to be consistent among different morphing methods, we select the same morphing pairs as in [30] in our experiments. Each face image is pre-processed following FFHQ [18] for fair comparison.

Evaluation Metrics. To evaluate the threat of each morphing attack to FRs, the mated morph presentation match rate (MMPMR) [31] based on the decision threshold at the false match rate (FMR) of 0.1% is employed. Specifically, the thresholds are calculated on the LFW dataset.

$$MMPMR(\tau) = \frac{1}{M} \cdot \sum_{m=1}^M \{ [\min_{n=1, \dots, N_m} S_m^n] > \tau \}, \quad (9)$$

where M and N_m denote the number of morphed images and contributing images, respectively. S_m^n is the similarity score for mated morph for morph m of the n -th subject, and τ is the threshold of the FRS at a chosen FMR. Obviously, the larger the MMPMR indicates stronger threat of the morphs.

The performance of different morphing attack detection (MAD) algorithms is measured by the Attack Presentation Classification Error Rate (APCER, the proportion of attack images misclassified as bona fide images) and the Bona fide Presentation Classification Error Rate (BPCER, the proportion of bona fide images misclassified as attack images) [34]. As it is impossible to optimize both APCER and BPCER jointly, we report results for APCER at specific BPCER values (1%, 5%, 10%, 20%) and for BPCER at specific APCER values (1%, 5%, 10%, 20%). In addition, when APCER is equal to BPCER, the Equal Error Rate (EER) is also reported.

To quantify the visual quality of morphed images, we follow [38] and [1] to use the Fréchet Inception Distance (FID), Structural Similarity Index (SSIM) and Peak Signal-to-Noise Ratio (PSNR) metrics. The FID metric measures the distance between the distribution of morphing attack images and the distribution of bona fide images used for the morphing attack. We use pytorch-fid [33] to compute FID. A lower FID means a closer resemblance between the distribution of generated morphing attack images and bona fide images, indicating higher visual fidelity [20].

C. Analysis on Results

Vulnerability of FRs. We investigate the vulnerability of four state-of-the-art FR models, FaceNet [32], ArcFace [12], CurricularFace [14] and ElasticFace-Arc [3], to morphing attacks. The former two FRs use the official pre-trained

TABLE II

DETECTION RESULTS OF MAD METHODS MIXFACE NET (MFN) AND HRNET (HRN) ON FERET DATASET. BOTH MODELS ARE TRAINED ON THE SMDD DATASET. HIGHER IS BETTER.

MAD	Method	EER (%)	APCER(%)@BPCER =				BPCER(%)@APCER =			
			1%	5%	10%	20%	1%	5%	10%	20%
MFN [17]	FaceMorpher [28]	9.64	44.23	16.07	8.32	2.27	24.15	16.23	8.68	4.15
	OpenCV [21]	13.23	65.97	36.67	23.06	6.81	38.87	21.32	15.85	11.13
	StyleGAN2 [35]	24.76	82.80	65.41	50.42	30.24	77.36	55.28	41.89	29.62
	MIPGAN-II [38]	30.81	79.21	63.52	53.31	39.51	83.39	65.09	45.66	35.28
	ReGenMorph [9]	11.91	43.86	20.79	10.59	1.70	24.72	15.47	11.13	5.47
	MorDIFF [8]	37.81	92.44	81.85	70.89	55.20	86.60	75.28	66.23	50.19
	HGFM (Ours)	39.31	96.03	88.85	79.21	63.89	90.19	74.91	66.04	54.34
HRN [15]	FaceMorpher [28]	10.02	70.32	28.17	9.83	0.76	19.43	13.77	10.00	6.23
	OpenCV [21]	14.18	86.77	48.96	27.98	4.72	32.26	20.00	16.04	12.07
	StyleGAN2 [35]	28.54	93.38	78.07	68.81	44.42	100.0	100.0	44.15	33.58
	MIPGAN-II [38]	23.06	89.79	69.56	54.06	32.14	100.0	100.0	38.11	26.41
	ReGenMorph [9]	8.88	73.72	25.52	6.81	0.76	19.62	12.64	8.68	6.04
	MorDIFF [8]	34.78	96.03	86.77	77.32	59.92	100.0	100.0	100.0	43.40
	HGFM (Ours)	35.54	99.43	90.37	82.41	65.03	100.0	100.0	100.0	46.04

TABLE III

DETECTION RESULTS OF MAD METHODS MIXFACE NET (MFN) AND HRNET (HRN) ON FRLL DATASET.

MAD	Method	EER (%)	APCER(%)@BPCER =				BPCER(%)@APCER =			
			1%	5%	10%	20%	1%	5%	10%	20%
MFN [17]	FaceMorpher [28]	2.29	2.29	1.72	1.23	0.65	13.24	1.47	1.47	1.47
	OpenCV [21]	1.97	2.29	1.31	0.98	0.66	12.75	0.49	0.49	0.49
	StyleGAN2 [35]	12.85	56.55	29.54	15.96	6.96	50.98	26.96	15.69	6.86
	MIPGAN-II [38]	2.21	9.17	1.80	1.39	1.23	30.88	2.45	0.49	0.49
	ReGenMorph [9]	1.15	1.06	0.25	0.16	0.16	1.47	1.47	1.47	1.47
	MorDIFF [8]	6.97	45.04	11.24	4.68	3.12	59.80	8.33	4.90	2.94
	HGFM (Ours)	12.78	76.58	34.56	16.72	7.53	77.94	32.35	16.18	7.35
HRN [15]	FaceMorpher [28]	0.98	0.90	0.49	0.33	0.24	0.98	0.49	0.49	0.49
	OpenCV [21]	1.31	1.31	0.82	0.49	0.24	4.41	0.49	0.49	0.49
	StyleGAN2 [35]	13.67	38.62	25.23	20.46	7.77	42.65	24.51	16.67	8.80
	MIPGAN-II [38]	9.57	23.57	16.84	11.14	3.37	45.10	15.69	10.29	2.94
	ReGenMorph [9]	8.94	3.19	0.24	0.24	0.08	2.45	2.45	2.45	0.00
	MorDIFF [8]	0.33	3.19	1.06	0.66	0.16	6.37	0.49	0.49	0.49
	HGFM (Ours)	11.96	37.18	25.47	18.59	8.35	53.43	27.45	15.20	8.82

TABLE IV

DETECTION RESULTS OF MAD METHODS MIXFACE NET (MFN) AND HRNET (HRN) ON FRGC DATASET.

MAD	Method	EER (%)	APCER(%)@BPCER =				BPCER(%)@APCER =			
			1%	5%	10%	20%	1%	5%	10%	20%
MFN [17]	FaceMorpher [28]	75.41	100.0	99.89	99.69	97.72	100.0	98.97	98.77	97.13
	OpenCV [21]	71.72	100.0	99.79	99.48	95.95	100.0	98.97	97.54	95.69
	StyleGAN2 [35]	83.19	100.0	99.79	99.27	98.23	100.0	100.0	100.0	99.59
	MIPGAN-II [38]	65.43	99.78	96.72	94.97	87.09	100.0	100.0	100.0	98.91
	ReGenMorph [9]	1.23	45.67	16.05	9.87	12.3	30.49	15.85	13.41	2.44
	MorDIFF [8]	3.94	83.15	64.99	48.58	24.94	66.59	38.65	32.53	23.14
	HGFM (Ours)	73.14	100.0	99.56	98.91	95.40	100.0	100.0	99.34	97.60
HRN [15]	FaceMorpher [28]	8.19	69.09	16.29	7.26	1.56	100.0	13.11	7.58	4.30
	OpenCV [21]	7.88	63.17	10.79	3.53	1.14	100.0	8.20	5.33	3.48
	StyleGAN2 [35]	6.64	42.32	8.30	4.05	0.52	19.26	8.20	4.30	2.46
	MIPGAN-II [38]	9.41	35.01	12.03	8.75	2.19	100.0	13.54	8.30	2.62
	ReGenMorph [9]	1.23	24.69	0.00	0.00	0.00	3.66	2.44	2.44	1.22
	MorDIFF [8]	3.94	20.35	2.19	0.00	0.00	7.42	3.71	1.75	1.09
	HGFM (Ours)	0.88	1.31	0.00	0.00	0.00	1.31	0.87	0.87	0.65

models and the latter two FRSS use ResNet100 as backbone trained on MS1MV dataset. To facilitate a more effective comparison of the methods in this paper, apart from the four previously mentioned morphing methods, we have also replicated two innovative morphing methods, ReGenMorph [9] and MorDIFF [8], using the official code provided to us. As tabulated in Table I, our HGFM achieves the highest MMPMR in most cases compared to other morphing

methods. This is primarily attributed to the local networks capturing information that the global network overlooks, effectively bridging the information gap. Additionally, the combined identity and geometry losses effectively preserve the identity of contributing individual faces, resulting in more threatening morphed images.

Detectability of Morphing Attacks. To measure the detectability of our method and other baselines, we deploy

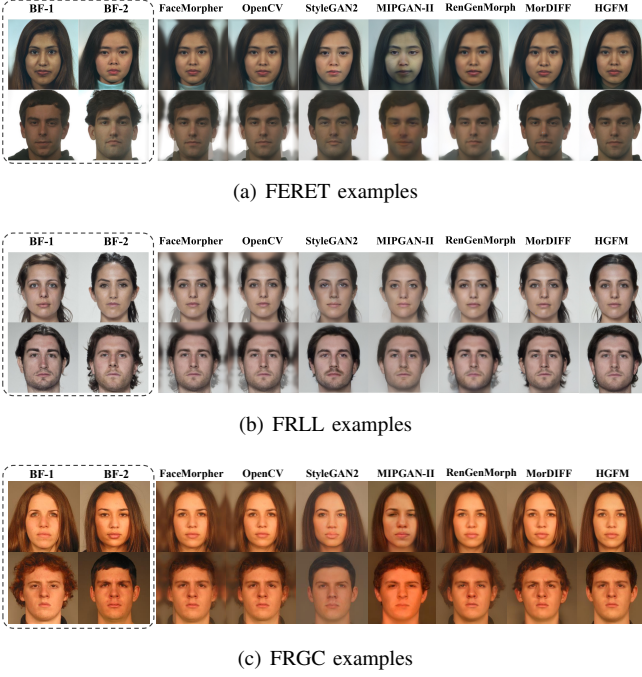


Fig. 3. Examples of morphs generated by different morphing attack methods on three benchmarks. Please zoom in to see the differences among the images, especially in regions susceptible to artifacts such as the eyes, nose, mouth, and hair.

two well-performing MAD algorithms, MixFaceNet [17] and HRNet [15]. Both of them all ranked high in the SYN-MAD 2022 [15] competition. Lacking public code for HRNet, we train it on the SMDD dataset following the same strategy and parameters of [17]. For MixFaceNet, we utilize the official model for testing. Table II presents the morphing attack (detectability) results on the FERET dataset. Notably the training and test sets of the MADs are disjoint, consistent with the cross-dataset evaluation in realistic scenarios. Among all morphing methods, our HGFM ranks first against the detection methods MixFaceNet and HRNet. This indicates that our method outperforms existing state-of-the-art morphing methods in multiple attack scenarios. The detection results for the FRLL dataset are available in Table III. The results on FRGC [24] dataset, which is well-known for its rich image variations in illumination and expression are presented in Table IV. The results show that our method performs poorly. We guess that the relatively poor MAD detection performance of our HGFM is because our current method is tailored for ICAO compliant images, but not very robust to image variations [1,30,40]. Additionally, experiments on the quantitative detection of morphed images by human observers are available in the Supplementary Material.

Visual Quality Assessments. The visual appearance of morphed images is essential, which determines whether it can successfully deceive human observers. As shown in Table I, our method, though is not the best in terms of image quality, is comparable to the best counterpart methods. More importantly, it is significantly better than existing methods in terms of attack success rate. Hence, our method

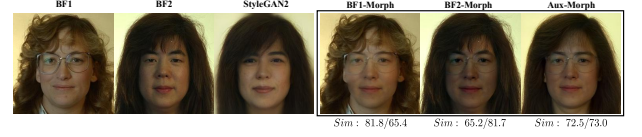


Fig. 4. Comparison of different blending schemes. From left to right: The two contributing images (BF1 and BF2), the auxiliary image generated by StyleGAN2, the morphed images generated via image blending using BF1 and BF2 simultaneously, using BF1 and BF2 sequentially, and using the StyleGAN2-generated auxiliary image. As the similarity (*Sim*) scores suggest, the last blending scheme achieves more balanced identity preservation between the two contributing subjects.

is superior in terms of the overall performance. As illustrated in Fig. 3, landmark-based morphs exhibit noticeable artifacts around the hair and face, while GAN-based morphs have excessively smooth faces and lack texture details. While ReGenMorph [9] exhibits higher SSIM and PSNR values, it is noteworthy that its FID values are considerably higher compared to our method (lower FID values indicate better performance). And ReGenMorph shows blurred facial areas and ghost morphs. Conversely, the latest SOTA method MorDIFF [8] morphs reproduce some facial details well, but there are strange artifacts in the hair area and red spots on the face of individual samples. This makes them susceptible to detection. In contrast, the morphed images generated by our method look much more realistic with less artifact. This is achieved by refining different facial regions separately using local morph networks and eliminating artifacts in areas outside the face with a mask-guided image blending module. In addition, the landmark morphed images provide pixel-level supervision and balance geometry and appearance information from both contributors.

D. Different artifact removal strategies

To provide a better explanation for using StyleGAN2-generated images as auxiliary images for image blending in **Stage-II**, we use the Poisson image blending [26] method to simulate the mask-guided image blending module. We perform image blending using one of the contributing images. As depicted in Fig. 4, when directly using the contributing image 1 for background replacement, the resulting morphed image becomes more similar to contributing subject 1 and significantly less identical to contributing subject 2. This significantly reduces the performance of morphs and is inconsistent with the intention of the face morphing attacks. On the other hand, due to the varying size of the face region in the intermediate morphing image and the contributing images, a significant skin tone inconsistency occurs at the articulation of the face region and the neck using the Poisson image blending method (See Fig. 4 and Fig. 5 (e)). As mentioned above, instead of using the original contributing images, we employ StyleGAN2 morphs as background images. Moreover, the Poisson image blending method cannot simultaneously optimize the blended image and the generated intermediate morphed image. It also has limitations and drawbacks, relying on precise boundary information and incurring high computational overhead. In contrast, our HGFM introduces a mask-guided image blending module to

TABLE V

DETECTABILITY OF MORPHED IMAGES WITH HRNET MAD ALGORITHM ON FERET DATASET. THE FIRST ROW INDICATES THAT NO GEOMETRY LOSS FROM (3) IS EMPLOYED, THE SECOND ROW INDICATES THAT ONLY ARCFACE [12] IS USED TO CALCULATE THE IDENTITY LOSS, THE THIRD ROW SHOWS THAT NO LOCAL NETWORKS (INCLUDING G_{l*} AND D_{l*}) AND LOCAL LOSS FROM (6) ARE USED, THE FOURTH ROW INDICATES THAT NO MASK-GUIDED IMAGE BLENDING MODULE AND MASK LOSS FROM (5), AND THE FIFTH ROW INDICATES THE REPLACEMENT OF MASK-GUIDED IMAGE BLENDING WITH THE POISSON IMAGE BLENDING [26] METHOD.

MAD	Method	EER (%)	APCER(%)@BPCER =				BPCER(%)@APCER =			
			1%	5%	10%	20%	1%	5%	10%	20%
HRN [15]	HGFM (w/o geometry)	35.35	99.05	90.36	81.66	64.65	100.0	100.0	100.0	18.74
	HGFM (w/ ArcFace)	35.53	99.05	89.98	82.23	64.84	100.0	100.0	100.0	46.23
	HGFM (w/o local)	35.53	98.86	89.79	82.41	63.71	100.0	100.0	100.0	19.28
	HGFM (w/o blending)	9.45	72.40	29.11	8.88	0.76	20.57	13.02	9.62	6.23
	HGFM (w/ poisson)	34.24	99.05	90.24	82.34	64.11	100.0	100.0	100.0	47.55
	HGFM	35.54	99.43	90.37	82.42	65.03	100.0	100.0	100.0	46.04

TABLE VI

COMPARISONS OF FID AND MMPMR@FMR=0.1% VALUES WITH DIFFERENT COMPONENTS ON FERET DATASET.

Method	FID↓	MMPMR (%)↑			
		FN [32]	AF [12]	CF [14]	EF [3]
HGFM (w/o geometry loss)	40.7	58.9	84.1	92.4	88.6
HGFM (w/ ArcFace)	41.1	57.1	84.3	92.4	87.9
HGFM (w/o local nets)	38.1	50.5	77.7	88.1	81.1
HGFM (w/o blending)	50.6	58.4	68.4	92.6	86.2
HGFM (w/ poisson)	44.7	53.4	64.0	89.0	82.4
HGFM	40.5	59.9	85.8	93.4	88.9

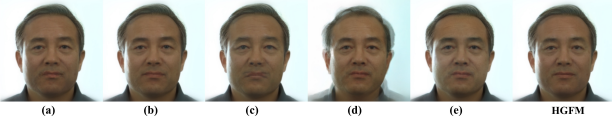


Fig. 5. Morphed images generated by different variants of our HGFM method in the ablation study. (a) Without geometry loss, (b) Without combined identity loss, (c) Without local morph network and local loss, (d) Without mask-guided blending, and (e) Using Poisson blending instead. Texture degradation, poor geometry and lighting preservation, ghosting, blurring, and unnatural features can be observed in these results, respectively.

mitigate the morphed image artifacts, ensuring the consistent facial region size between the intermediate morphed image and the background image.

E. Ablation Study

To investigate the effect of different modules of HGFM on morphing generation, we conduct an ablation study on FERET dataset. Specifically, we focus on four major components: (i) the geometry loss, (ii) the combined identity loss, (iii) the local networks, and (iv) the mask-guided image blending module. Table VI shows the performance of the ablation study quantified using MMPMR and FID values. The qualitative results are shown in Fig. 5. Quantitative results on MAD algorithms are given in Table V. According to the results, four conclusions can be summarized as follows.

Firstly, using multiple pre-trained FR models to extract identity features enhances the identity preservation capability and the generalization ability of the morphed images against unknown FRs. Secondly, supervision using an additional landmark-based morphed image is helpful to improve the visual quality of the morphed image along with the attack capability of FRs. Thirdly, although there are still edge

artifacts when combining local face patches using minimum pooling to resolve overlapping regions, the local networks effectively capture detailed information related to identity and refine local regions' facial texture. This significantly improves the attack performance. Fourthly, the mask-guided image blending module overcomes the issue of excessive color penetration from the intermediate morphed image into the auxiliary morphed image (background image), which can lead to loss of morphed content. It also produces a more natural and harmonious skin tone along the facial contour. As a result, artifacts are effectively removed, improving overall image quality.

V. CONCLUSIONS

This paper introduces HGFM, a new architecture for generating high-quality and high identity-preserving morphed images. The core of the proposed HGFM is the hierarchical generative network, which extracts detailed and consistency information of contributing images separately. HGFM combines the identity loss and geometry loss in the model optimization process, resulting in enhanced attack capability of morphed images against both known and unknown FRs. HGFM also conceives a mask-guided image blending module to eliminate noticeable artifacts in areas outside the face to improve the visual quality further. To evaluate the attack potential of the proposed method, we have compared it with representative landmark-based and generation-based morphing methods to assess the visual quality of morphing images, identity preservation, and detection performance against the MAD algorithms. Quantitative and qualitative results show that HGFM performs better in preserving identity and visual quality than other methods.

In future work, we will explore the refinement of the morphing network to extract global and local information more efficiently from both contributing images, and more effective strategies for combining the two types of information to generate higher-quality morphs.

REFERENCES

- [1] Z. Blasingame and C. Liu. Diffusion models for stronger face morphing attacks. *arXiv preprint arXiv:2301.04218*, 2023.
- [2] G. Borghi, A. Franco, G. Graffieti, and D. Maltoni. Automated artifact retouching in morphed images with attention maps. *IEEE Access*, 9:136561–136579, 2021.

- [3] F. Boutros, N. Damer, F. Kirchbuchner, and A. Kuijper. Elasticface: Elastic margin loss for deep face recognition. In *Proceedings of the IEEE/CVF Conference on Computer Vision and Pattern Recognition*, pages 1578–1587, 2022.
- [4] S. Cao, X. Liu, X. Mao, and Q. Zou. A review of human face forgery and forgery-detection technologies. *Journal of Image and Graphics*, 27(4):1023–1038, 2022.
- [5] L.-C. Chen, G. Papandreou, F. Schroff, and H. Adam. Rethinking atrous convolution for semantic image segmentation. *arXiv preprint arXiv:1706.05587*, 2017.
- [6] R. Chen, X. Chen, B. Ni, and Y. Ge. Simswap: An efficient framework for high fidelity face swapping. In *Proceedings of the 28th ACM International Conference on Multimedia*, pages 2003–2011, 2020.
- [7] N. Damer, F. Boutros, A. M. Saladié, F. Kirchbuchner, and A. Kuijper. Realistic dreams: Cascaded enhancement of gan-generated images with an example in face morphing attacks. In *2019 IEEE 10th International Conference on Biometrics Theory, Applications and Systems (BTAS)*, pages 1–10. IEEE, 2019.
- [8] N. Damer, M. Fang, P. Siebke, J. N. Kolf, M. Huber, and F. Boutros. Mordiff: Recognition vulnerability and attack detectability of face morphing attacks created by diffusion autoencoders. *arXiv preprint arXiv:2302.01843*, 2023.
- [9] N. Damer, K. Raja, M. Süßmilch, S. Venkatesh, F. Boutros, M. Fang, F. Kirchbuchner, R. Ramachandra, and A. Kuijper. Regenmorph: Visibly realistic gan generated face morphing attacks by attack regeneration. In *Advances in Visual Computing: 16th International Symposium, ISVC 2021, Virtual Event, October 4-6, 2021, Proceedings, Part I*, pages 251–264. Springer, 2021.
- [10] N. Damer, A. M. Saladié, A. Braun, and A. Kuijper. Morgan: Recognition vulnerability and attack detectability of face morphing attacks created by generative adversarial network. In *2018 IEEE 9th International Conference on Biometrics Theory, Applications and Systems (BTAS)*, pages 1–10, 2018.
- [11] L. DeBruine and B. Jones. Face research lab london set, 2017.
- [12] J. Deng, J. Guo, N. Xue, and S. Zafeiriou. Arcface: Additive angular margin loss for deep face recognition. In *Proceedings of the IEEE/CVF conference on computer vision and pattern recognition*, pages 4690–4699, 2019.
- [13] Q. He, Z. Deng, Z. He, and Q. Zhao. Optimal-landmark-guided image blending for face morphing attacks. In *2023 IEEE International Joint Conference on Biometrics (IJCB)*, pages 1–9. IEEE, 2023.
- [14] Y. Huang, Y. Wang, Y. Tai, X. Liu, P. Shen, S. Li, J. Li, and F. Huang. Curricularface: adaptive curriculum learning loss for deep face recognition. In *proceedings of the IEEE/CVF conference on computer vision and pattern recognition*, pages 5901–5910, 2020.
- [15] M. Huber, F. Boutros, A. T. Luu, K. Raja, R. Ramachandra, N. Damer, P. C. Neto, T. Gonçalves, A. F. Sequeira, J. S. Cardoso, et al. Synmad 2022: Competition on face morphing attack detection based on privacy-aware synthetic training data. In *2022 IEEE International Joint Conference on Biometrics (IJCB)*, pages 1–10. IEEE, 2022.
- [16] P. Isola, J.-Y. Zhu, T. Zhou, and A. A. Efros. Image-to-image translation with conditional adversarial networks. In *Proceedings of the IEEE conference on computer vision and pattern recognition*, pages 1125–1134, 2017.
- [17] M. Ivanovska, A. Kronovšek, P. Peer, V. Štruc, and B. Batagelj. Face morphing attack detection using privacy-aware training data. *arXiv preprint arXiv:2207.00899*, 2022.
- [18] T. Karras, S. Laine, and T. Aila. A style-based generator architecture for generative adversarial networks. In *Proceedings of the IEEE/CVF conference on computer vision and pattern recognition*, pages 4401–4410, 2019.
- [19] Z. Ke, J. Sun, K. Li, Q. Yan, and R. W. Lau. Modnet: Real-time trimap-free portrait matting via objective decomposition. In *Proceedings of the AAAI Conference on Artificial Intelligence*, pages 1140–1147, 2022.
- [20] M. Lucic, K. Kurach, M. Michalski, S. Gelly, and O. Bousquet. Are gans created equal? a large-scale study. *Advances in neural information processing systems*, 31, 2018.
- [21] S. Mallick. Opencv-based morph. <https://learnopencv.com/2016>.
- [22] F. Matteo, F. Annalisa, and M. Davide. The magic passport. In *IEEE International Joint Conference on Biometrics (IJCB'14)*, pages 1–7, 2014.
- [23] M. Pernuš, V. Štruc, and S. Dobrišek. High resolution face editing with masked gan latent code optimization. *arXiv preprint arXiv:2103.11135*, 2021.
- [24] P. J. Phillips, P. J. Flynn, T. Scruggs, K. W. Bowyer, J. Chang, K. Hoffman, J. Marques, J. Min, and W. Worek. Overview of the face recognition grand challenge. In *2005 IEEE computer society conference on computer vision and pattern recognition (CVPR'05)*, volume 1, pages 947–954. IEEE, 2005.
- [25] P. J. Phillips, H. Wechsler, J. Huang, and P. J. Rauss. The feret database and evaluation procedure for face-recognition algorithms. *Image and vision computing*, 16(5):295–306, 1998.
- [26] T. Porter and T. Duff. Compositing digital images. In *Proceedings of the 11th annual conference on Computer graphics and interactive techniques*, pages 253–259, 1984.
- [27] L. Qin, F. Peng, S. Venkatesh, R. Ramachandra, M. Long, and C. Busch. Low visual distortion and robust morphing attacks based on partial face image manipulation. *IEEE Transactions on Biometrics, Behavior, and Identity Science*, 3(1):72–88, 2020.
- [28] A. Quek. Facemorpher. <http://www.facemorpher.com>, 2019.
- [29] R. Raghavendra, K. Raja, S. Venkatesh, and C. Busch. Face morphing versus face averaging: Vulnerability and detection. In *2017 IEEE International Joint Conference on Biometrics (IJCB)*, pages 555–563. IEEE, 2017.
- [30] E. Sarkar, P. Korshunov, L. Colbois, and S. Marcel. Vulnerability analysis of face morphing attacks from landmarks and generative adversarial networks. *arXiv preprint arXiv:2012.05344*, 2020.
- [31] U. Scherhag, A. Nautsch, C. Rathgeb, M. Gomez-Barrero, R. N. Veldhuis, L. Spreuwers, M. Schils, D. Maltoni, P. Grother, S. Marcel, et al. Biometric systems under morphing attacks: Assessment of morphing techniques and vulnerability reporting. In *2017 International Conference of the Biometrics Special Interest Group (BIOSIG)*, pages 1–7. IEEE, 2017.
- [32] F. Schroff, D. Kalenichenko, and J. Philbin. Facenet: A unified embedding for face recognition and clustering. In *Proceedings of the IEEE conference on computer vision and pattern recognition*, pages 815–823, 2015.
- [33] M. Seitzer. “pytorch-fid: Fid score for pytorch,” version 0.2.1. <https://github.com/mseitzer/pytorch-fid>, 2020.
- [34] S. Venkatesh, R. Ramachandra, K. Raja, and C. Busch. Face morphing attack generation and detection: A comprehensive survey. *IEEE transactions on technology and society*, 2(3):128–145, 2021.
- [35] S. Venkatesh, H. Zhang, R. Ramachandra, K. Raja, N. Damer, and C. Busch. Can gan generated morphs threaten face recognition systems equally as landmark based morphs? – vulnerability and detection, 2020.
- [36] T.-C. Wang, M.-Y. Liu, J.-Y. Zhu, A. Tao, J. Kautz, and B. Catanzaro. High-resolution image synthesis and semantic manipulation with conditional gans. In *Proceedings of the IEEE conference on computer vision and pattern recognition*, pages 8798–8807, 2018.
- [37] R. Yi, Y.-J. Liu, Y.-K. Lai, and P. L. Rosin. Apdrawinggan: Generating artistic portrait drawings from face photos with hierarchical gans. In *Proceedings of the IEEE/CVF conference on computer vision and pattern recognition*, pages 10743–10752, 2019.
- [38] H. Zhang, S. Venkatesh, R. Ramachandra, K. Raja, N. Damer, and C. Busch. Mipgan—generating strong and high quality morphing attacks using identity prior driven gan. *IEEE Transactions on Biometrics, Behavior, and Identity Science*, 3(3):365–383, 2021.
- [39] K. Zhang, Z. Zhang, Z. Li, and Y. Qiao. Joint face detection and alignment using multitask cascaded convolutional networks. *IEEE signal processing letters*, 23(10):1499–1503, 2016.
- [40] N. Zhang, X. Liu, X. Li, and G.-J. Qi. Morphganformer: Transformer-based face morphing and de-morphing. *arXiv preprint arXiv:2302.09404*, 2023.